Silver Nano Particle-Containing Inorganic–Organic Hybrid via Sol–Gel Synthesis

Ming-Shien Yen*
Department of Materials Engineering, Kun Shan University, Tainan 71003, Taiwan

Abstract

Inorganic–organic hybrids containing silver nanoparticles (Ag NPs) were synthesized with silica and thiazole azo dye by a sol–gel process using vinyltriethoxysilane (VTES) as a precursor. The materials were synthesized from tetraethoxysilane (TEOS) with thiazole azo dyes, which in turn were synthesized using 2-amino thiazole as the coupling component that underwent a coupling reaction with the diazonium component, p-nitroaniline. Alternatively, the thiazole azo dyes were processed by the hydrolysis-condensation reaction with constant ratios of VTES and TEOS in appropriate proportions using a catalyst, followed by the incorporation of various ratios of Ag NPs. The structures of these hybrid materials were examined by Fourier transform infrared analysis, ^{29}Si nuclear magnetic resonance spectroscopy, X-ray diffraction, and energy-dispersive X-ray spectroscopy.

Keywords

Ag NPs, silica, thiazole dyes, hybrid materials

I. INTRODUCTION

Most new products are designed to have multiple functions and a form of intelligence. Thus, hybrid materials have recently become one of the main trends in materials science research. Compared to traditional materials, the most important feature of a hybrid material is its designability. The mechanical, physical, and chemical properties of a hybrid material can be designed and controlled by changing its composition or using interface control, compounding technology, or molding technology to meet the requirements of maximum usability and environmental compatibility [1–3]. Organic–inorganic hybrid materials contain both organic and inorganic functionalities and provide functional compensation and optimization [4–8]. Consequently, they are widely used in numerous fields including optics, catalysis, and in other biomaterials.

Nanoparticles possess great application potential because of their surface properties that are different from those of bulk materials. Such properties make it possible to endue ordinary products with new functionalities. Metallic nanoparticles have many functions such as heterogeneous catalysts, antibacterial activity, photocatalytic activity, optical switching devices, gas sensors, optical waveguides, and electrochemical biosensors [9–16]. Among the metal nanoparticles, silver nanoparticles (Ag NPs) are considered desirable and effective in many fields. In order to produce highly effective nanoparticles, several synthesis methods have been used based on some common approaches such as physical processes of atomization or milling, chemical methods such as chemical reduction, biological irradiation, photocatalytic activity, and green synthesis methods [17–23].

Furthermore, silica is a natural material derived from common materials such as quartz, sand, and flint. Silica has high chemical stability, a low thermal expansion coefficient, and high heat resistance. The relatively high chemical stability of the silica phase can be advantageous in some cases [24–27]. Among the metals, silver owing to its unusual physicochemical properties and biological activities. Moreover, if silver and silica gels are sufficiently intermixed within the surface layer of a material during the condensation polymerization process, the short travelling distance between the surface-modified silica sites, which offer thermal stability, and the silver sites, which offer antimicrobial.

The molecules of heteroaryl azo dyes contain unshared electron pairs of nitrogen and sulphur that can easily trigger resonance and cause the excitation of π electrons of the compound from the ground state to the excited state. The synthesis and spectroscopic properties of azo dyes are well-established [28–32]. Moreover, the use of heterocyclic aromatic amines to improve the tinctorial strength is well known.

Modern industries and consumers desire multifunctional products; therefore, multifunctioning organic–inorganic hybrid materials have become popular. The sol–gel method is a frequently used organic–inorganic hybrid material preparation method that combines inorganic and organic molecular networks [33–36]. Ag NPs are a powerful antimicrobial agent that deactivates several microorganisms [37]. Extensive studies are being conducted on Ag NPs for their antibacterial efficacy and may have potential commercial application areas such as medical tools, appliances, and healthcare products [38]. The doping of Ag NPs in a matrix,

which was subsequently incorporated in other organic materials to create hybrid materials that are widely used to produce various chemical products. In the present work, Ag NPs have been combined with a siloxane network to increase the additive effect, thereby obtaining antimicrobial capability and superhydrophobicity. Subsequently, the sol–gel method was applied to prepare organic–inorganic hybrid dyes, which yielded hybrid materials exhibiting a network structure consisting of the processed dye, vinyltriethoxysilane (VTES)/Ag NPs, and VTES/TEOS/Ag NPs through additive hydrolysis. This will enable the use of hybrid dyes during the processing of high molecular products.

II. EXPERIMENT

A) Analytical Instruments

Fourier-transform infrared (FT-IR) spectra were recorded on a Bio-Rad Digilab FTS-40 spectrometer (KBr); 1H nuclear magnetic resonance (NMR) spectra were obtained on a BRUKER AVANCE 400MHz NMR spectrometer. Chemical shifts (δ) are expressed in parts per million using tetramethylsilane (TMS) as an internal standard. The ^{29}Si-NMR spectra were collected using a BRUKER AVANCE 400 MHz NMR spectrometer at 78.49 MHz, with a recycle time of 60 s, and the number of scans was 914. The elemental analysis was carried out using a Philips XL40 FEG-Energy Dispersive X-ray Spectrometer. X-ray diffraction (XRD) measurements were performed on a Rigaka D/MAX 2500V X-ray powder diffractometer in steps of 0.01° using Cu Kα radiation as the X-ray source.

B) Materials

Vinyltriethoxysilane (VTES), tetraethoxysilane (TEOS), p-nitroaniline, polyvinylpyrrolidone (PVP), and acetophenone were purchased from Acros Co., Ltd., Belgium, and thiourea, sulfuric acid, silver nitrate, glucose, and iodide were purchased from Hayashi Pure Chemical Ind., Ltd., Japan.

C) Preparation of dye 5-[2-(4-nitrophenyl)-diazen-1-yl]-4-phenyl-1,3-thiazol- 2-amine (3)

A finely ground powder of *p*-nitroaniline **2** (1.38 g, 0.01 mol) was added to hydrochloric acid (12 mL) and stirred for 20 min. Sodium nitrite (0.72 g, 0.0105 mol) was added in portions to concentrated sulphuric acid (5 mL) at 10°C and stirred for 1 h at 60–65°C. The solution was cooled to below 5°C, and then the finely ground derivatives were slowly added; the mixture was stirred for an additional 1 h at 5–10°C until it was clear. The resulting diazonium solution was used immediately in the coupling reaction. A clear mixed solution of the coupling component 4-phenyl-2-aminothiazole **1** (2.0 g, 0.01 mol) and 10% sodium carbonate was stirred. The diazonium mixture was added at 0–5°C, and the solution was stirred for at least 2 h; it was diluted to raise its pH to 5–6 (by adding aqueous sodium hydroxide or sodium acetate). The resulting product was filtered, washed with water, and re-crystallized from ethanol to give a deep red solid, 5-[2-(4-nitrophenyl)-diazen-1-yl]- 4-phenyl-1,3-thiazol-2-amine (**3**) (2.3 g, 70%). M.P. 245-247°C; Fourier transform infrared (FTIR) (KBr)/cm^{-1}: 3433 (NH_2), 3057 (C–H); ^{1}H NMR (DMSO-d_6) δ ppm: 7.04 (1H, s, –NH_2), 7.51–7.55 (5H, m, ArH), 7.71, (2H, d, 2,6- Ph–H), 8.19 (2H, d, 3,5- Ph–H). $C_{15}H_{17}N_2O_2S$ (325.1) Calcd.: C, 55.38; H, 3.41; N, 21.53; O, 9.84; S, 9.85. Found: C, 55.32; H, 3.44; N, 21.58; O, 9.78; S, 9.87.

D) Preparation of precursor 5-[2-(4-nitrophenyl)-diazen-1-yl]-4-phenyl-N-[2- (triethoxysilyl)ethyl]-1,3- thiazol-2-amine (4)

Precursor **4** was prepared by the reaction of dye **3** (3.25 g, 0.01 mol) followed by the addition of VTES (9.5 g, 0.05 mol) in ethanol (80 mL) with stirring at 65°C for 4 h at an adjusted pH of 4–5. The resulting product was filtered, washed with water, and re-crystallized from ethanol to give a dark red solid, 5-[2-(4-nitrophenyl)-diazen-1-yl]-4-phenyl-N-[2-(triethoxysil- yl)ethyl]-1,3-thiazol-2- amine (**4**) (2.76 g, 59%). M.P. 304–306°C; FTIR (KBr)/cm^{-1}: 3395 (NH), 3073 (C–H), 1096 (O–Si). $C_{23}H_{29}N_5O_5SSi$ (515.4) Calcd.: C, 53.57; H, 5.67; N, 13.58; O, 15.51; S, 6.22; Si, 5.45. Found: C, 53.63; H, 5.62; N, 13.56; O, 15.55; S, 6.28; Si, 5.41.

E) Preparation of Ag NPs

$AgNO_3$ (1.7 g) was added dropwise into de-ionized water (8.5 mL) and glucose (3.6 g) was added as a reducing agent under magnetic stirring to prepare the solution. Then, PVP (2 g) as a stabilizer for the produced nanosilver was dissolved into de-ionized water (25.5 mL) and mixed with the prepared solution under magnetic stirring at ambient temperature. Few drops of 10% sodium hydroxide were added under stirring to adjust the pH of the solution to 11–12. The reaction was carried out for 15 min with constant stirring at 60 °C. The brown color of the solution indicated the formation of Ag NPs.

F) Synthesis of hybrid materials

As shown in Scheme 1, Precursor **4** and the prepared Ag NP solution were mixed in a fixed ratio. To this was added 0.01 mol of hydrochloric acid and 10 mL of water to maintain a pH level of 3–4. The mixture was then placed in a thermostat stirrer and heated under reflux for 4 h to facilitate condensation reaction for the production of hybrid material. We changed the concentration of Ag NPs in the prepared solution doped with TEOS to attain varying degrees of polycondensation reaction and obtain hybrid materials 5 and 6.

G) Preparation of hybrid materials

Hybrid material **P_1** was prepared by the condensation of precursor **4** (5.01 g, 0.01 mol) and the prepared Ag NP solution (0.01 mol) in ethanol (80 mL) by stirring at 65 °C for 2 h with the addition of hydrochloric acid (0.365 g, 0.01 mol) and water (5 mL). Hybrid materials **P_2–P_4** were synthesized using the same method as that used for synthesizing **P_1**; however, the molar ratios of precursor **4** to the Ag NPs were 1:1, 1:1.5, 1:2, and 1:2.5 for the hybrid materials **P_1–P_4,** respectively. Hybrid material **Q_1** was prepared by the condensation of precursor **4** (5.01 g, 0.01 mol), TEOS (4.16 g, 0.025 mol), and Ag NP solution (0.025 mol) in ethanol (80 mL) under stirring at 65 °C for 2 h by adding hydrochloric acid (0.365 g, 0.01 mol) and water (5 mL). The **Q** series of hybrid materials were synthesized using the same method but with different molar ratios of precursor **4** to TEOS in hydroly- sis polycondensation at a constant ratio of Ag NPs; the molar ratios of precursor **4**:TEOS:Ag NPs were 1:2.5:2.5, 1:5:2.5, 1:7.5:2.5, and 1:10:2.5 for **Q_1–Q_4,** respectively.. Hybrid material **R_1** was prepared by the condensation of precursor **4** (5.01 g, 0.01 mol), TEOS (4.16 g, 0.1 mol), and Ag NP solution (0.01 mol) in ethanol (80 mL) under stirring at 65 °C

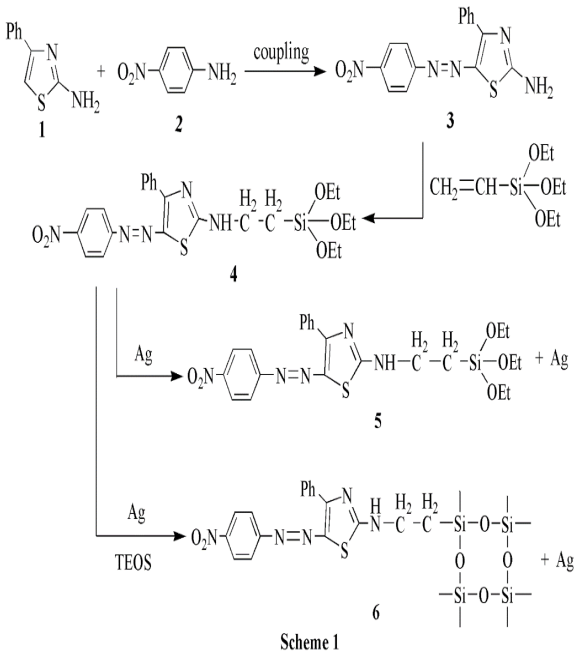

Scheme 1 Synthesis of hybrid material 5, 6

for 2 h by adding hydrochloric acid (0.365 g, 0.01 mol) and water (5 mL). The **R** series of hybrid materials were prepared by the same method but with different the molar ratios of precursor **4** to Ag NPs in hydrolysis polycondensation at a constant ratio of TEOS; the molar ratios of precursor **4**:TEOS:Ag NPs were 1:10:1, 1:10:1.5, 1:10:2, and 1:10:2.5 for **R_1–R_4**, respectively.

III. RESULTS AND DISCUSSION

A) FTIR analysis

The FTIR spectra of the dyes and hybrid materials indicate that dye **3** has absorption peaks corresponding to the N–H and C–H groups at 3332 and 2972 cm^{-1}, respectively. In the FTIR spectrum of precursor **4**, an obvious shift in the amino group absorption peak close to 3424 cm^{-1}, which is typically found at 3418 cm^{-1}, suggests partial reaction of the dye with VTES. The appearance of the Si–OR absorption peak around 1074 cm^{-1} proves that VTES could convert the primary amine group into a secondary amine group; the resultant absorption peak appeared around 3380 cm^{-1}. These results indicate reactions between some of the dyes and VTES. The FTIR spectrum of hybrid material **6** includes the absorption peak of the converted secondary amine. The intense signal corresponding to the Si–O group at 1100 cm^{-1} proves the dissociation of the NH_2 moiety. The Si–C bond, which gave rise to the peak at 1244 cm^{-1}, reveals that the dissociation of NH_2 bond is followed by bonding with CH_2, resulting in the linkage of the Si–O bonds to form Si–O–Si network.

Figure 1 shows the FT-IR spectra of hybrid materials **P_1–P_4**. An absorption peak corresponding to the vibrations of the benzene ring appeared near 1652 cm^{-1} and that for the Si–O group appeared near 1109 cm^{-1}; in both the cases, the absorption strength increased with Ag concentration. Therefore, the Ag content further completes the bonding of precursor. Figure 2 shows the FT-IR spectra of hybrid materials **Q_1–Q_4**. The intensity of the Si–O group absorption peak near 1091 cm^{-1} increased as the TEOS concentration increased, indicating that the formation of network structure increased with TEOS concentration. Figure 3 shows the FT-IR spectra of hybrid materials **R_1–R_4**. The N–H group absorption peak at 3431 cm^{-1}, the benzene group absorption peak near 1641 cm^{-1}, and the Si–O group absorption peak near 1072 cm^{-1} increased with Ag concentration; however, the increase in peak intensity was obvious for the N–H group and small for the Si–O group.

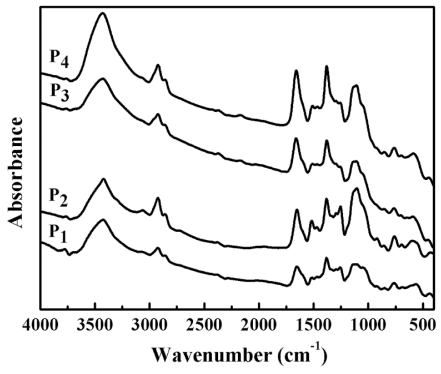

Fig. 1 FT-IR spectra of hybrid materials P_1–P_4

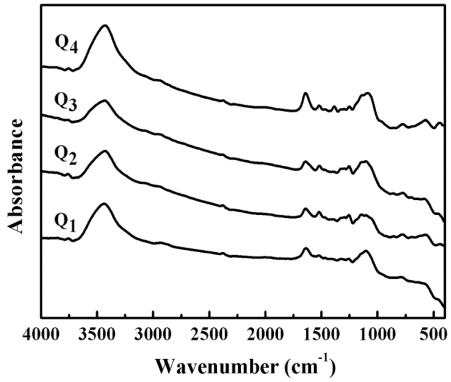

Fig. 2 FT-IR spectra of hybrid materials Q_1–Q_4

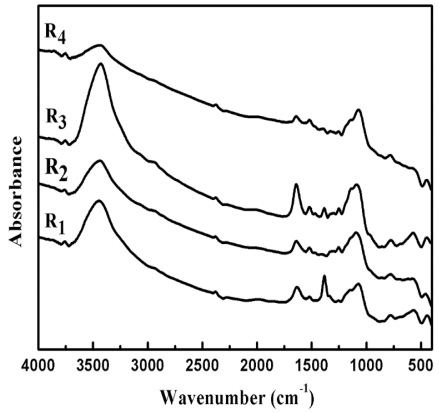

Fig. 3 FT-IR spectra of hybrid materials R_1–R_4

B) ^{29}Si NMR spectra analysis

^{29}Si NMR is often used to characterize the structures formed by Si hydrolysis. While the FTIR results above indicated the formation of Si–O–Si bonds by a sol–gel reaction, the solid-state ^{29}Si NMR provided additional information on the structure of silica and the extent of the Si–OH condensation reaction [39]. The T^3, Q^3, and Q^4 absorption peaks were located by applying ^{29}Si NMR spectroscopy. Figure 4 shows that the ^{29}Si NMR spectra of the simple dye and VTES contain absorption peaks at ~69.56 ppm (T^2) and ~80.71 ppm (T^3), corresponding to Si–OR formation following the hydrolysis of VTES. Figure 5 shows the ^{29}Si NMR spectra of the processed hybrid dye formed with various proportions of VTES and TEOS. Peaks appeared at ~101.06 ppm (Q^3) owing to absorption by (H–O)Si(–OSi≡)$_3$ structures and at ~108.91 ppm (Q^4) due to the absorption by Si(–OSi≡)$_4$ structures. The structure of the Si–OR absorption peak indicated that some Si quadruple bonds had an unreacted Si–OH functional group, (H–O)Si(–OSi≡)$_3$, and some Q^3 quadruple bonds had an unreacted Si–O functional group, Si(–OSi≡)$_3$. The structure of Q^4 indicates that the Si quadruple bond reacted completely with the Si–O functional group, Si(–OSi≡)$_4$.

The ^{29}Si NMR spectrum of hybrid material $\mathbf{P_2}$ prepared by polycondensation reaction of precursor **4** with a fixed ratio Ag NPs, according to the results in Figure 4, showed a relatively significant noise peak and an obvious T^3 absorption peak at δ=78.89 ppm. This indicates that the hybrid material existed as R–Si(–OSi≡)$_3$, that is, the hybrid material did not formed Si–O–Si network structure. The ^{29}Si NMR spectrum of the hybrid material prepared with a fixed ratio of Ag NPs and different concentrations of TEOS, according to the results in Figure 5, forming a network structure showed Q^3 and Q^4 absorption peaks besides the T^3 absorption peak. In the spectra of hybrid materials $\mathbf{Q_1}$–$\mathbf{Q_4}$, T^3 absorption occurred near δ=79.51 ppm, and the absorption peak intensity decreased as the TEOS concentration increased. Therefore, the increase in concentration led to the formation of Si–O–Si network structure of the hybrid material, with a decrease in the R–Si(–OSi≡)$_3$ structure and the T^3 absorption peak. The absorption peak Q^3 appeared near δ=99.29 ppm for the hybrid materials $\mathbf{Q_1}$ and $\mathbf{Q_2}$, but disappeared gradually as the concentration increased. Moreover, only the Q^4 absorption peak appeared near δ=110.03 ppm as the TEOS concentration increased, which led to a decrease in its noise peak, thereby yielding a smooth peak; this implied that the Si–O–Si network structure of the hybrid material was completely formed.

C) Energy-dispersive X-ray spectra analysis

The energy-dispersive X-ray spectroscopy **(**EDS) analysis results are presented in Table 1 and Figures 6 and 7. When additional Ag NPs were added to the hybrids $\mathbf{P_1}$–$\mathbf{P_4}$, the quantity of Si decreased with increasing Ag concentration. As shown in Table 1 and Figures 8 and 9, the hybrids $\mathbf{Q_1}$–$\mathbf{Q_4}$ had a fixed molar concentration of Ag NPs and a moderately increasing molar concentration of TEOS. EDS analysis showed that the increasing TEOS concentration increased the Si content in the hybrid materials, and thus, the Ag concentration decreased gradually. In hybrid materials $\mathbf{R_1}$–$\mathbf{R_4}$, according to the results in Table 1, Figure 10, and Figure 11, the Ag content increased with Ag addition.

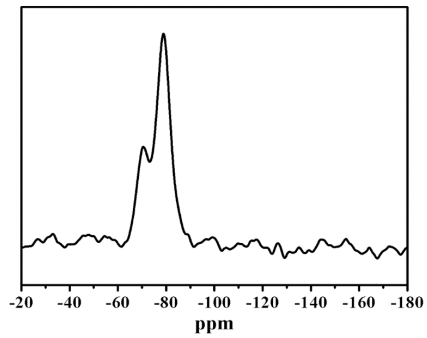

Fig. 4 ^{29}Si-NMR spectra of hybrid material P_3

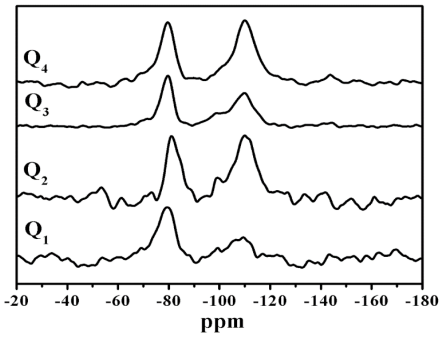

Fig. 5 ^{29}Si-NMR spectra of hybrid materials Q_1–Q_4

Table 1: EDS analysis of hybrid materials P_1–P_4, Q_1–Q_4, and R_1–R_4

Samples	Elemental composition (%)				
	C	O	S	Si	Ag
P_1	57.54	15.18	2.21	12.7	12.37
P_2	53.39	13.42	2.08	11.82	19.29
P_3	48.47	12.12	1.87	9.08	28.46
P_4	46.28	10.65	1.76	7.63	33.68
Q_1	47.36	15.21	1.89	18.95	16.59
Q_2	44.28	19.54	1.72	21.63	12.83
Q_3	39.81	21.54	1.51	26.39	10.75
Q_4	33.79	23.29	1.25	34.12	7.55
R_1	34.42	23.69	1.83	35.24	4.82
R_2	33.68	22.94	1.64	34.25	7.49
R_3	31.75	22.16	1.62	33.57	10.90
R_4	30.71	21.59	1.51	32.54	13.65

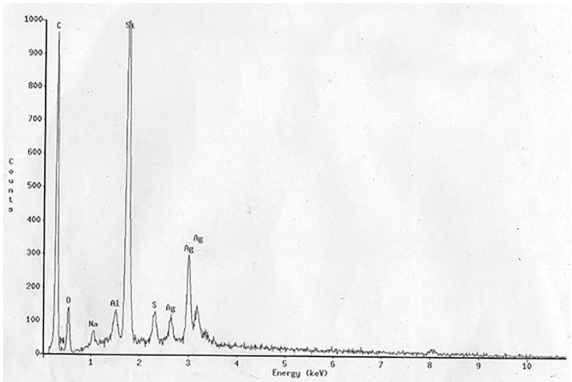

Fig. 6 The EDS diagram of hybrid materials P_1

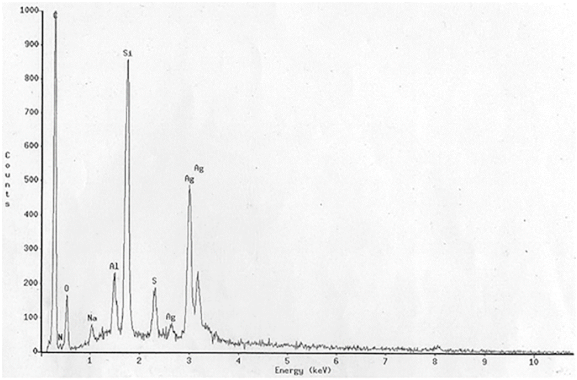

Fig. 7 The EDS diagram of hybrid materials P_4

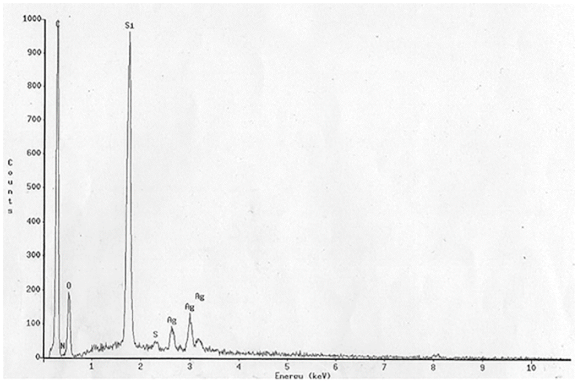

Fig. 8 The EDS diagram of hybrid materials Q_1

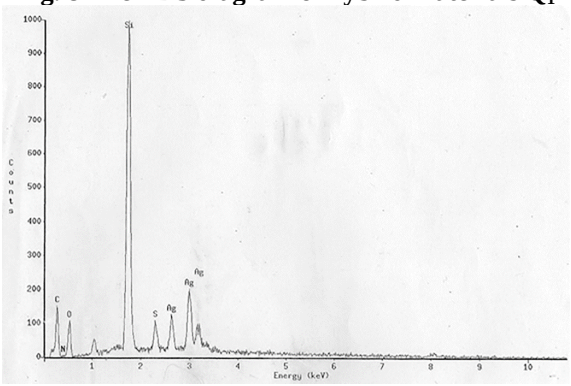

Fig. 9 The EDS diagram of hybrid materials Q_4

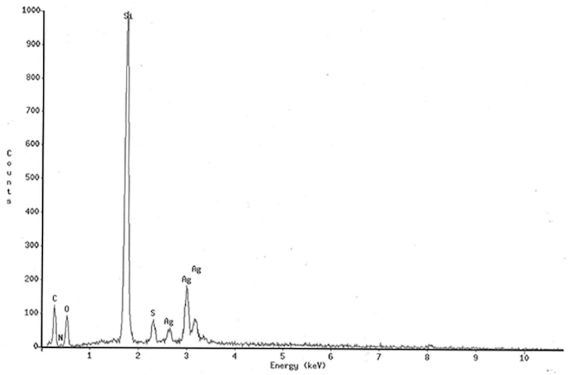

Fig. 10 The EDS diagram of hybrid materials R_1

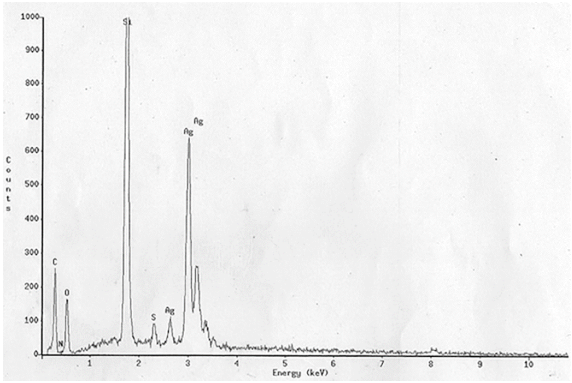

Fig. 11 The EDS diagram of hybrid materials R_4

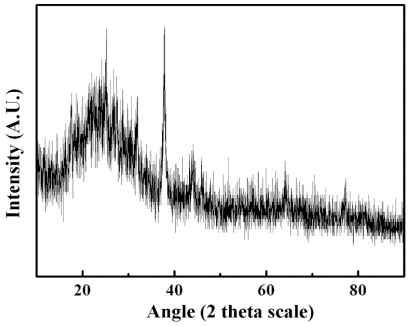

Fig. 13 The XRD diagram of hybrid materials Q_4

D) X-Ray diffraction analysis

In this study, we analyzed the hybrid materials in the **Q_4** and the unsintered Ag powder developed by a sol–gel process (hereafter, Ag powder) by X-ray diffraction (XRD). Because neither the series of hybrid materials nor the Ag powder was sintered, all these materials exhibited amorphous structures without clear crystal phases, as shown in Figures 12 and 13. Figure 12 shows the XRD spectrum of Ag crystal structure, with the prominent peaks at 2θ = 38.12°, 44.32°, 64.46°, 77.40° and 81.54° corresponding to the (111), (200), (220), (311), and (222) Bragg's reflections of an FCC crystal structure, respectively [40]. Figure 13 shows the light diffraction analysis of hybrid material **Q_4** prepared with precursor **4**, TEOS, and Ag NPs, in which the diffraction peaks appeared at 2θ = 25°, 38.12°, 44.32°, 64.46°, 77.40°, and 81.54°. The diffraction peak near 2θ = 25° may be the diffraction peak of the dye, while the other diffraction peaks correspond to Ag metal in the hybrid material, approximately matching the data from literature. The noise peaks in the spectrum of the hybrid material arose because the dye has an amorphous structure and the diffraction peak is not obvious.

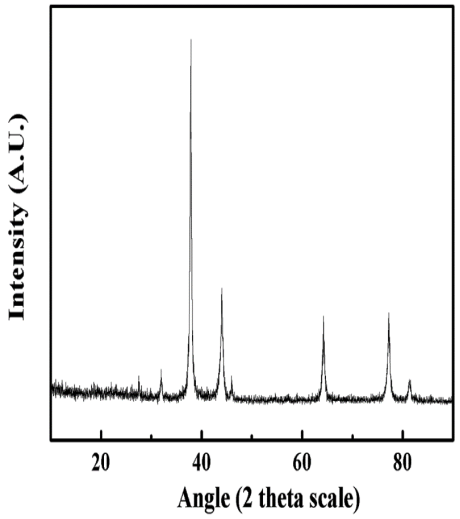

Fig. 12 The XRD diagram of Ag NPs

IV. CONCLUSIONS

This study focused primarily on the sol–gel synthesis of a series of heterocyclic thiazole dyes with various proportions of added VTES/Ag NPs and VTES/TEOS/Ag NPs. The derived hybrids were further analyzed to understand their chemical and physical properties. FTIR analysis showed that the absorption peak of the Si–O–Si functional group appeared in the range of 1072 to 1109 cm^{-1}, which confirmed the formation of network structure. In the ^{29}Si NMR analysis, the Q^3 peak appeared near δ=99.29 ppm for the hybrid materials **Q_1** and **Q_2**, but disappeared gradually as the concentration increased. Moreover, only the Q_4 absorption peak appeared near δ=110.03 ppm as the TEOS concentration increased. In addition, the EDS results showed that when additional Ag NPs were added to the hybrids **R_1**–**R_4**, the Ag NPs content increased, leading to a continuous decrease in the Si content. Further, the diffraction peaks of Ag in hybrid material **Q_4**, appeared at 2θ = 25°, 38.12°, 44.32°, 64.46°, 77.40°, and 81.54°, respectively.

ACKNOWLEDGMENT

The authors thank the Ministry of Science and Technology of the Republic of China, Taiwan, for financially supporting this research under grant MOST 105-2221-E-168-029.

REFERENCES

[1] D. C. Clive, R. Christophe, and J. H. S. Mark, "Chemical aspects of solution routes to perovskite-phase mixed-metal oxides from metal-organic precursors," *Chem. Rev.*, vol. 93, pp. 1205–1241, 1993.

[2] D. A. Loy, and K. J. Shea, "Bridged polysilsesquioxanes highly porous hybrid organic- inorganic materials," *Chem. Rev.*, vol. 95(5), pp. 1431–1442, 1995.

[3] J. D. Mackenzie, "Structures and properties of ormosils," *J. Sol-Gel Sci. Technol.*, vol. 2(1-3), pp. 81–86, 1994.

[4] F. Hoffmann, M. Cornelius, J. Morell, and M. Fröba, "Silica-Based Mesoporous Organic–Inorganic Hybrid," *Angew. Chem. Int. Ed.*, vol. 45, pp. 3216–3251, 2006.

[5] C. Sanchez, B. Julián, P. Belleville, and M. Popall, "Applications of hybrid organic–inorganic nanocomposites," *J. Mater. Chem.*, vol. 15, pp. 3559–3592, 2005.

[6] P. Judeinstein ,and C. Sanchez, "Hybrid organic inorganic materials a land of multidisciplinarity," *J. Mater. Chem.*, vol. 6(4), pp. 511–525, 1996.

[7] Y. H. Han, A. Taylor, M. D. Mantle, and K. M. Knowles, "Sol–gel-derived organic–inorganic hybrid materials," *J. Non-Cryst. Solids.*, vol. 353, pp. 313–320, 2007.

[8] R. D. Maggio, S. Dirè, E. Callone, F. Girardi, and G. Kickelbick, "Hybrid organic–inorganic materials using zirconium based NBBs and vinyl trimethoxysilane: Effect of pre-hydrolysis of silane," *Polymer*, vol. 51, pp. 832–841, 2010.

[9] G. C. Bond, "The Origins of Particle Size Effects in Heterogeneous Catalysis," *Surf. Sci.*, vol. 156, pp. 966–981, 1985.

[10] S. Ahmed, M. Ahmad, B. L. Swami, and S. Ikram, "A review on plants extract mediated synthesis of silver nanoparticles for antimicrobial applications A green expertise," *J. Adv. Res.*, vol. 7, pp. 17–28, 2016.

[11] F. Gonella, G. Mattei, and P. Mazzoldi, "Structural and Optical Properties of Silver-Doped," *Chem. Mater.*, vol. 11, pp. 814–821, 1999.

[12] M. V. Roldán, A. Frattini, O. de Sanctis, H. Troiani, and N. Pellegri, "Characterization and applications of Ag nanoparticles in waveguides," *Appl. Surf. Sci.*, vol. 254, pp. 281–285, 2007.

[13] S. Shrivastava, T. Bera, A. Roy, G. Singh, P. Ramachandrarao and D. Dash, "Characterization of enhanced antibacterial effects of novel silver nanoparticles," *Nanotechnology*, vol. 18, 225103–225111, 2007.

[14] Y. L. Liu, H. F. Yang, Y. Yang, Z. M. Liu, G. L. Shen, and R. Q. Yu, "Gas sensing properties of tin dioxide coated onto multi-walled carbon nanotubes," *Thin Solid Films*, vol. 497, pp. 355–360, 2006.

[15] J. Dong, Y. Wen, Y. Miao, Z. Xie, Z. Zhang, and H. Yang, "A nanoporous zirconium phytate film for immobilization of redox protein and the direct electrochemical biosensor," *Sensor Actuator B*, vol. 150, pp. 141–147, 2010.

[16] G. Mitrikas, Y. Deligiannakis, C. C. Trapalis, N. Boukos, and G. Kordas, "CW and Pulsed EPR Study of Silver Nanoparticles in a SiO_2 Matrix," *J. sol–gel Sci. Tech.*, vol. 13, pp. 503–508, 1998.

[17] R. Dastjerdi, and M. Montazer, "A review on the application of inorganic nano-structured materials in the modification of textiles: Focus on antimicrobial properties," *Colloid. Surf. B*, vol. 79, pp. 5–18, 2010.

[18] H. M. Sung-Suh, J. R. Choi, H. J. Hah, S. M. Koo, and Y. C. Bae, "Comparison of Ag deposition effects on the photocatalytic activity of nanoparticulate TiO_2 under visible and UV light irradiation," *J. Photochem. Photobiolo. A*, vol. 163, pp. 37–44, 2004.

[19] V. K. Sharma, R. A. Yngard, and Y. Lin, "Silver nanoparticles: Green synthesis and their antimicrobial activities," *Adv. Colloid Interface Sci.*, vol. 145, pp. 83–96, 2009.

[20] W. K. Son, J. H. Youk, and W. H. Park, "Antimicrobial cellulose acetate nanofibers containing silver nanoparticles," *Carbohyd. Polym.*, vol. 65, pp. 430–434, 2006.

[21] K. Vimala, K. S. Sivudu, Y. M. Mohan, B. Sreedhar, and K. M. Raju, "Controlled silver nanoparticles synthesis in semi-hydrogel networks of poly(acrylamide) and carbohydrates: A rational methodology or antibacterial application," *Carbohyd. Polym.*, vol. 75, pp.463–471, 2009.

[22] B. Zhao, and Y. W. Chen, "Ag/TiO_2 sol prepared by a sol–gel method and its photocatalytic activity, *J. Phys. Chem. Solids*, vol. 72, pp. 1312–1318, 2011.

[23] S. G. Balwe, V. V. Shinde, A. A. Rokade, S. S. Park, and Y. T. Jeong, "Green synthesis and characterization of silver nanoparticles (Ag NPs) from extract of plant Radix Puerariae: An efficient and recyclable catalyst for the construction of pyrimido[1,2-b]indazole derivatives under solvent-free conditions," *Cataly. Commun.*, vol. 99, pp. 121–126, 2017.

[24] W. Zhou, J. E. Mark, M. R. Unroe, and F. E. Arnold, "Toughening of a high-temperature polymer by the sol–gel, in situ generation of a rubbery silica–siloxane phase," *J. Appl. Polym. Sci.*, vol. 79, pp. 2326–2330, 2001.

[25] N. D. Hegde, and A. V. Rao, "Physical properties of methyltri-methoxysilane based elastic silica aerogels prepared by the two-stage sol–gel process," *J. Mater. Sci.*, vol. 42, pp. 6965–6971, 2007.

[26] Y. Dimitriev, Y. Ivanova, and R. Iordanova," History of sol–gel science and technology," *J. Univ. Chem. Technol. Metall.*, vol. 43(2), pp. 181–192, 2008.

[27] X. Du, and J. He, "A self-templated etching route to surface-rough silica nanoparticles for superhydrophobic coatings," *ACS Appl. Mater. Interfaces*, vol. 3, pp. 1269–1276, 2011.

[28] M. S. Yen, and I. J. Wang, "Synthesis and Absorption Spectra of Hetarylazo Dyes derived from Coupler 4-Aryl-3-Cyano-2-Aminothiophenes," *Dyes Pigm.*, vol. 61, pp. 243–250, 2004.

[29] A. D. Towns, "Developments in azo disperse dyes derived from heterocyclic diazo components," *Dyes Pigm.*, vol. 42, pp. 3–28, 1999.

[30] G. Hallas, and A. D. Towns, "A comparison of the properties of some 2-aminothiophene-derived disperse dyes," *Dyes Pigm.*, vol. 31, pp. 273–289, 1996.

[31] I. Zadrożna, and E. Kaczorowska, "Synthesis and characteristics of azo chromophores for nonlinear-optical application," *Dyes Pigm.*, vol. 71, pp. 207–211, 2006.

[32] M. S. Yen, and I. J. Wang, "A facile syntheses and absorption characteristics of some monoazo dyes in bis-heterocyclic aromatic systems part II: syntheses of 4-(p-substituted) phenyl-2- (2-pyrido-5-yl and 5-pyrazolo-4-yl) azo-thiazole derivatives," *Dyes Pigm.*, vol. 63, pp. 1–9, 2004.

[33] S. Pandey, and S. B. Mishra, "Sol–gel derived organic–inorganic hybrid materials synthesis, characterizations and applications," *J. Sol-Gel Sci. Technol.*, vol. 59, pp. 73–94, 2011.

[34] K. H. Wua, C. I. Liu, C. C. Yang, G. P. Wang, and C. M. Chao, "Preparation and characterization of aminosilane-modified silicate supported with silver for antibacterial behaviour," *Mater. Chem. Phys.*, vol. 125, pp. 802–806, 2011.

[35] Y. S. Shin, M. Park, H. Y. Kim, F. L. Jin, and S. J. Park, "Synthesis of Silver-doped Silica-complex Nanoparticles for Antibacterial Materials," *Bull. Korean Chem. Soc.*, Vol. 35(10), pp. 2979–2984, 2014.

[36] O. Akhavan, and E. Ghaderi, "Bactericidal effects of Ag nanoparticles immobilized on surface of SiO_2 thin film," *Curr. Appl. Phys.*, vol.9, pp. 1381–1385, 2009.

[37] M. Nassar, and A. M. Youssef, "Mechanical and antibacterial properties of recycled carton paper coated by PS/Ag nanocomposites for packaging," *Carbohyd. Polym.*, vol. 89, pp. 269–274, 2012.

[38] M. Kawashita, S. Tsuneyama, F. Miyaji, T. Kokubo, H. Kozuka, K. Yamamoto, "Antibacterial silver-containing silica glass prepared by sol-gel method," *Biomaterials*, vol. 21, pp. 393–398, 2000.

[39] R. J. Hook, "A 29Si-NMR study of the sol–gel polymerisation rates of substituted ethoxysilanes," *J. Non-Cryst. Solids*, vol. 195, pp. 1–15, 1996.

[40] P. Shetty, N. Supraja, M. Garud, and T. N. V. K. V. Prasad, "Synthesis, characterization and antimicrobial activity of Alstonia scholaris bark-extract-mediated silver nanoparticles," *J. Nanostruct. Chem.*, vol. 4, pp. 161–170, 2014.